Acta Cryst. (1976). A32, 823

The Role of Multiple Scattering in the Study of Lattice Images of Graphitic Carbons

BY D. A. JEFFERSON, G. R. MILLWARD* AND J. M. THOMAS

Edward Davies Chemical Laboratories, University College of Wales, Aberystwyth, Dyfed SY23 1NE, Wales

(*Received* 5 *March* 1976; *accepted* 12 *April* 1976)

The effect of multiple scattering upon the nature of the electron-microscope images of graphitic specimens has been investigated by theoretical calculations within the systematics multislice approach. For perfect, infinite specimens, imaged under axial illumination, the results agreed closely with those predicted by a simple three-beam dynamical treatment. In all cases the weak-phase-object approximation was found to be invalid, even qualitatively, whenever specimen thicknesses exceeded 50 Å. Calculations were also performed for finite crystal sizes and various plausible types of structurally imperfect graphites. The calculated images demonstrate the need for great care in interpreting experimental images of structurally defective graphitic solids. In particular, the positions of missing layers in a crystal of graphite can be 'filled' by spurious fringes under certain conditions of defocus, and fringes corresponding to layers of an intercalated species turn out to have ill defined positions. Characteristics such as these are equally prominent in all images, irrespective of the magnitude of multiple scattering, suggesting that these perturbations arise primarily from instrumental aberrations.

1. Introduction

Many attempts have been made to elucidate the ultrastructure of various kinds of graphitized carbons by high-resolution electron microscopy (Heidenreich, Hess & Ban, 1968; Fourdeux, Herinckx, Perret & Ruland, 1969; Ban, 1972; Evans, Jenkins & Thomas, 1972; Johnson & Crawford, 1973; Millward & Thomas, 1974; Crawford & Marsh, 1975). In some of these investigations (see, for example, Millward & Thomas, 1974) optical diffractometry has been used to correct for the transfer effects of the electron optical system, a procedure which relies on the assumption that the specimens behave as weak-phase objects, enabling linear transfer theory to be applied. The aim of the work summarized in this paper is to determine the magnitude of specimen thickness at which the weak-phase-object assumption is no longer valid; and also to investigate computationally the modifications manifested in the observed image as a result of multiple electron scattering. Discussion of the effects of chromatic aberration and partially coherent illumination upon modified images of this type are at present neglected; their influence will be considered in a subsequent publication.

2. Multislice calculations

Lattice images for a variety of graphitic specimens have been computed by the multislice method of Cowley & Moodie (1957*a*). The images corresponded to those from specimens, viewed along the layer planes, which were structurally perfect and of infinite extent along ⟨0001⟩, and also specimens of very limited extent which contained imperfections of various types. The instrumental factors of objective-lens spherical aberration and defect of focus (hereafter designated DF) were also taken into account in the calculation of the final images. As most of the graphitic carbons to which these calculations apply had been assumed to be essentially 'turbostratic' structures, lacking all correlation between layers other than an (approximately) constant spacing, the systematics approximation (Hoerni, 1956) was used in the multislice calculation. This greatly reduced the number of beams required in the calculation for the one-dimensionally perfect specimens, and enabled progress to be made with the computed images of various models of imperfect graphites (see below). However, any application of this treatment to a three-dimensionally crystalline graphite would certainly require the incorporation of a two-dimensional multislice calculation. All the calculations described below were carried out on a CDC 7600 computer up to a maximum specimen thickness of 1000 Å, and a slice thickness (Δz) of 5 Å was found to be adequate for this purpose. The inelastic scattering was neglected in all cases.

2.1. *Perfect one-dimensional graphitic systems*

The phases, amplitudes and intensities of 00l beams were calculated for one-dimensionally perfect, infinite crystals as a function of specimen thickness parallel to the layer planes, structure factors up to $l = \pm 20$ being used in the construction of the single slice phase grating, the transform of which was then evaluated up to $l = \pm 10$. The calculation routines were first checked against previously published data for the oxide $W_4Nb_{26}O_{77}$ (Lynch, 1974). Diffracted beam intensities for the situation of axial illumination are plotted as a function of specimen thickness in Fig. 1, the corresponding values for the case of tilted illumination being given in Fig. 2, the tilt being such that

* Walter Idris Jones Fellow.

the excitation errors of 000 and $00\bar{2}$ beams were identical. Final normalization of the intensities for the axial and tilted illumination cases was 0·99049 and 0·99343 respectively at a specimen thickness of 1000 Å.

For axial lllumination, the 000, $00\bar{2}$ and 002 beams show strong interference, with near-complete extinction of the 000 beam at a specimen thickness of approximately 105 Å. By comparison, 004 and $00\bar{4}$ are almost unaffected, but as their amplitude is at least one order of magnitude lower, it follows that the scattering from this type of graphite can be described almost exactly by a simple three-beam theory. Intensity plots for such a theory, with 000 and 002 amplitudes given by $\cos(\pi t/\xi g)$ and $(1/\sqrt{2})\sin(\pi t/\xi g)$ respectively, t being the total specimen thickness and ξ_g the appropriate extinction distance, are also shown in Fig. 1. The agreement between the two models is very good. The three-beam treatment gives a constant $\pm\pi/2$ phase difference between 000 and 002 beams, and the figure for the difference derived from the multislice treatment agrees closely with this value.

A similar comparison was made in the case of tilted illumination, with a two-beam model and an extinction distance twice that used in the axial case. Agreement was then much poorer, the calculated extinction distance for 000 being *ca* 130 Å from the multislice calculation and *ca* 210 Å from the two-beam model. In addition, the multislice calculation demonstrates that for tilted illumination the amplitudes of 002 and $00\bar{4}$ beams are by no means negligible, an essential assumption in the two-beam treatment. Some extent of the disparity between the two approaches may be judged from Fig. 2.

It therefore appears that for perfect, infinite specimens of graphite, diffracted beam amplitudes are severely affected by multiple scattering, even at crystal thicknesses of less than 100 Å, and that the weak-phase object approximation is severely limited in its formal application. The pronounced effect of multiple scattering is strikingly revealed in the nature of the calculated images: Fig. 3 shows a series of calculated images for specimen thicknesses of up to 300 Å, as a function

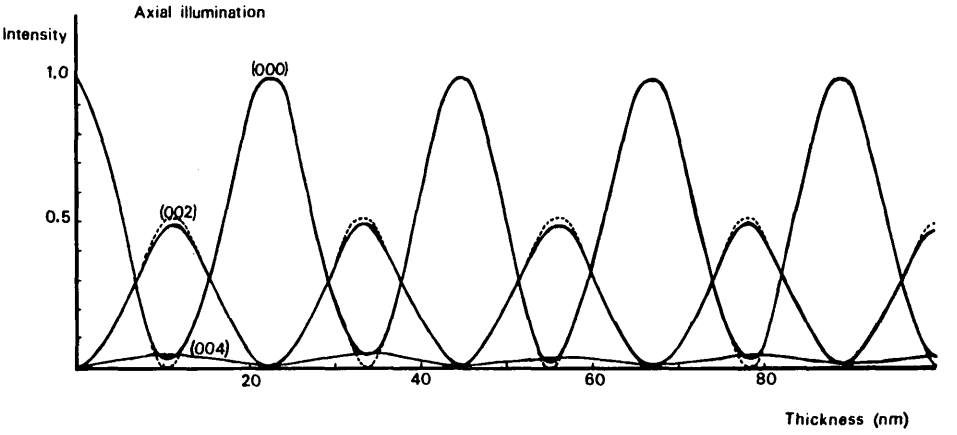

Fig. 1. 000, 002 and 004 diffracted beam intensities derived from a systematics multislice calculation (full lines) with axial illumination plotted as a function of specimen thickness. 000 and 002 beam intensities from a three-beam calculation (dashed lines) are shown for comparison.

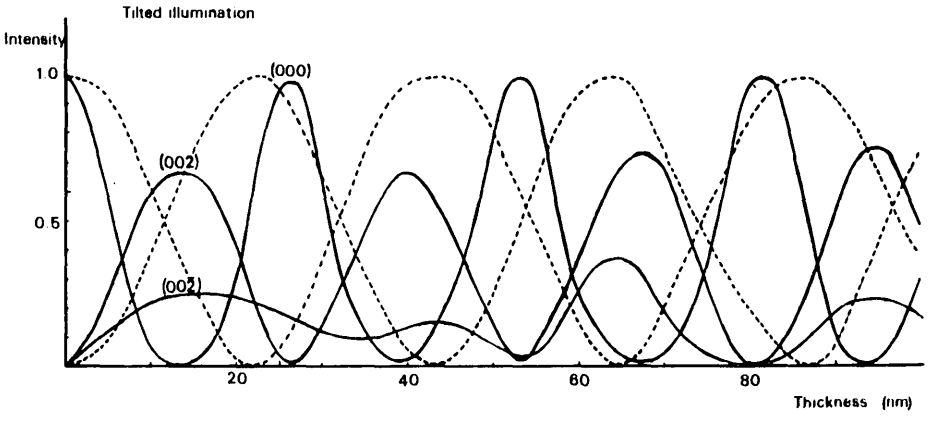

Fig. 2. 000, 002, $00\bar{2}$ and $00\bar{4}$ diffracted beam intensities from a systematics multislice (full lines) with tilted illumination. 000 and $00\bar{2}$ intensities from a two-beam calculation (dashed lines) are also shown.

of DF over the range 0 to 600 Å, and with a spherical aberration coefficient (C_s) of 1·6 mm. An objective aperture of radius 0·5 $Å^{-1}$ was included in the image calculation. The variation is approximately d^2/λ, which is the amount of defocus required to twice reverse contrast of the principal 3·4 Å spacing, so that the images at DF=0 and DF=600 Å will superimpose directly, these two images being Fourier images* (Cowley & Moodie, 1957*b*) of the structure. The strong 1·7 Å fringes in the image of a 100 Å thick specimen can be clearly seen, although they form only a minor part of the image contrast at other thicknesses. At thicknesses of less than 50 Å, the 1·7 Å component of the image is not observed. It is evident that, as the phase difference between 000 and 002 beams is approximately $\pm\pi/2$, the value required by the weak-phase object approximation, the approximation will be satisfied, at least qualitatively, up to 50 Å thickness, but will fall down in the range 50–100 Å.

2.2. *Structurally imperfect specimens*

The models discussed above apply only to perfect and infinite specimens of graphite, and require extension to embrace real systems involving crystals of limited size and/or structural perfection. For a one-dimensional model crystal (*i.e.* one again viewed along the layer planes but of limited extent along ⟨0001⟩ there will be a continuous range of scattering angles, so that a method of calculating dynamical amplitudes and phases for a continuous range of spatial frequencies is required. This, unfortunately, is at present computationally impracticable, but two possible approaches may be envisaged.

The simplest approach entails regarding the diffracted amplitude from a real crystal as the amplitude scattered by a perfect, infinite crystal convoluted with a function which depends upon crystal size and perfection. For thicker crystals, dynamical effects are allowed for by evaluating dynamical amplitudes for a perfect crystal, and then convoluting with the same crystal size/perfection function. For graphitic systems, the dynamical calculation can then be limited to a three-beam type (Hines, Imeson & Howie, 1975), but as the crystal size/perfection function is not involved in the dynamical calculation, contrast variations in the image arising from structural imperfections will be completely unaffected by increasing crystal thickness and will be altered only by variations in the operational DF values and the aberrations present.

The alternative, more rigorous approach includes the effect of imperfections into the dynamical calculation, requiring the ability to handle much larger numbers of beams. The multislice method can be adapted to such a model by considering finite dimensions of crystalline graphite, and constructing an artificial lattice where each unit cell contains one finite single crystal (Grinton & Cowley, 1971), with, on either side, completely empty regions. This model can then be multisliced, and if the disturbance in the wavefront produced by the graphitic region at the centre of one unit cell does not interact with that from neighbouring cells it will be satisfactory. Models of this type have been recently applied to complex oxide structures (MacLagan, Bursill & Spargo, 1975) and, with conventional many-beam methods, to single atom imaging (Spence, 1975).

Further precautions are, however, necessary when computing images from such models. Owing to the replacement of a finite object by an artificial periodic structure of repeat distance d_L (the dimension of the large unit cell), the image will naturally exhibit principal Fourier images at defocus intervals of $DF=d_L^2/\lambda$. Consequently, images from such a model can, at best, only be an approximation to the true image intensity, and this approximation will be progressively worse as DF becomes greater. For the electron microscope, with its relatively high spherical aberration, this will be further complicated by the fact that there is no single position of 'exact' focus for all spatial frequencies. However, for a unit cell of $d_L=100$ Å, the principal Fourier images will be separated by $DF=2{\cdot}7\times10^5$ Å, and within the limits of DF considered here ($0<DF<$ 2000 Å), the image will closely resemble that from a truly finite object. Nevertheless, it must be borne in mind that such approximate models become less exact at high values of DF, and also, if greater specimen thicknesses are employed, when interactions between adjacent cells become significant.

* In this study we have used the nomenclature of Fourier images given by Rogers (1969). For an object of periodicity d, principal Fourier images of the object will be separated by an amount of defocus $DF=d^2/\lambda$. If, however, the image of the object is synthesized from more than one pair of diffracted beams, there will be intermediate Fourier images separated by amounts of defocus $d^2/n\lambda$, which can carry more lines than the original structure. The nature of such images is especially important when considering the calculation of lattice images from crystals of limited extent (see § 2.2).

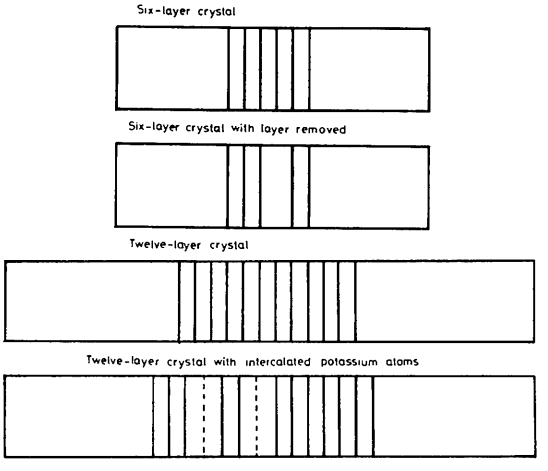

Fig. 4. Schematic drawings of the large unit cells used for calculating lattice images of finite and imperfect crystals.

The method discussed above is clearly more complicated than the simple picture of assuming that contrast effects from imperfections are unaffected by increasing crystal thickness, but it provides a more versatile approach to the problem. With the concept of a perfect crystal multiplied by a size/perfection function, calculations are restricted to cases of finite size and displacement disorders only, whereas with the large-cell method other effects, such as the occurrence of intercalated guest species within the graphite host, can be handled. Schematic drawings of the large unit cells used in the subsequent calculations are shown in Fig. 4.

2.3. *Models used*

Four distinct models were selected for theoretical assessment. (i) A perfect graphite crystal with six layers only. (ii) As (i), but with one layer removed. (iii) A perfect graphite crystal with 12 layers. (iv) As (iii), but with two layers of intercalated K atoms corresponding to a composition of $C_{48}K$.

For (i) and (ii) the calculation was initially undertaken for a unit cell of 66 Å dimension, containing six and five layers of graphite respectively. In each case the graphitic region, situated in the centre of the unit cell, was of 16·6 Å width, with a 24·7 Å empty margin at either side. The phase-grating transform of this cell was determined from structure factors out to $l = \pm 200$, the transform of the grating being determined out to $l = \pm 100$. The process was then repeated for a 110 Å cell, keeping the same graphitic regions but with the dimensions of the empty margins increased to 46·7 Å, and structure factors out to $l = \pm 330$ and $l = \pm 165$ to define the phase grating and its transform respectively. Results from these two models were compared, and within the limits DF = 0–2000 Å, the differences were marginal. Models (iii) and (iv) were calculated on the basis of the 110 Å unit cell. Spherical aberration coefficient and objective aperture sizes were again taken to be 1·6 mm and 0·5 $Å^{-1}$ respectively.

Images from the two different cells used for (i) are shown in Fig. 5, where the differences can be seen to be very slight. The 66 Å cell was therefore considered to give sufficient accuracy for both (i) and (ii). A complete range of images for (i) and (ii) is illustrated in Figs. 6 and 7, with the corresponding cell projected potential, which clearly shows the missing layer in (ii). Several striking features are observed in these images, one of which is that the DF interval between successive contrast reversals of the 3·4 Å spacing in the 50 Å thick case is no longer constant, but varies slightly with the magnitude of DF. This discrepancy is however very much less than that reported in experimental measurement of contrast reversal positions in graphites of undefined thickness (Crawford & Marsh, 1975). Owing to the severely limited extent of the graphitic region, the image detail contains ripples at the edge of this region which, particularly at certain values of DF, suggest the presence of additional graphitic layers. For the 50 Å thick six-layer crystal (Fig. 6*a*) possibly the best approximation to the actual crystal potential is observed at DF = 1700 Å, the next best being at 1100 Å. Both, however, contain extra fringes which could be mistaken for additional layers, and the positions of contrast reversal are even worse in this respect. The picture is more complicated in the 100 Å thick specimen, where the principal spacing is of the 1·7 Å type (as observed in the infinite crystal model), and the edges of the crystal become rather poorly defined. In (ii), where one layer is missing, fringe shifts and contrast reversal show even more remarkable effects. For the 50 Å thick specimen (Fig. 7*a*) the clearest indication of a missing layer is found in the image calculated for DF = 800 Å, but at this value the existing layers show poor contrast. At DF = 1100 Å, these layers are shown with distinctive contrast, but there is a spurious fringe in the position of the 'missing' layer, albeit with reduced contrast. A similar situation prevails at the next position of maximum 3·4 Å fringe contrast (1400 Å), but at subsequent positions (1700 and 2000 Å) the spurious fringe again appears to be present with maximum contrast. Further misleading effects arise in the 100 Å thick specimen, with no indication this time of a missing layer at any of the DF settings, except that at 800 Å. Evidently, electron-microscope observation of even so major a defect as a missing layer requires the greatest experimental care, with preferably, some form of through-focal series of exposures necessary to characterize it completely.

The calculated images for (iii) and (iv) are possibly more revealing in their consequences. Images for 50 Å thick specimens in each case are illustrated in Figs. 8 and 9. For a simple 12-layer graphite crystal (iii) there is a marked similarity to the results obtained for (i), there being an irregular DF interval between successive positions of maximum 3·4 Å fringe contrast, and an uncertainty in the number of layers in the crystal. With (iv) however, the obvious difficulty in locating the layers of K atoms emphasizes the complexity to be expected in interpreting images of graphite intercalated with other guest species. The crystal in (iv) is essentially that of (iii) with two layers of K atoms inserted between (counting from left to right) layers three and four and layers five and six of the 12-layer crystallite, this composition being equivalent to an overall stoichiometry of $C_{48}K$. The crystal in (iv) is also displaced to the right by one layer, so that layer 11 in (iv) is in the same position as layer 12 in (iii). As the layer of K atoms has a lower projected potential density than a graphite layer the image contrast at the former might be expected to be a fringe of reduced intensity and slightly larger spacing (3·8 instead of 3·4 Å). Of the calculated images, only that computed for DF = 800 Å shows clearly the reduced contrast at the positions of the K atoms. Moreover, around these positions, the contrast of the principal 3·4 Å fringes is also reduced. (At this defocus, layers of carbon

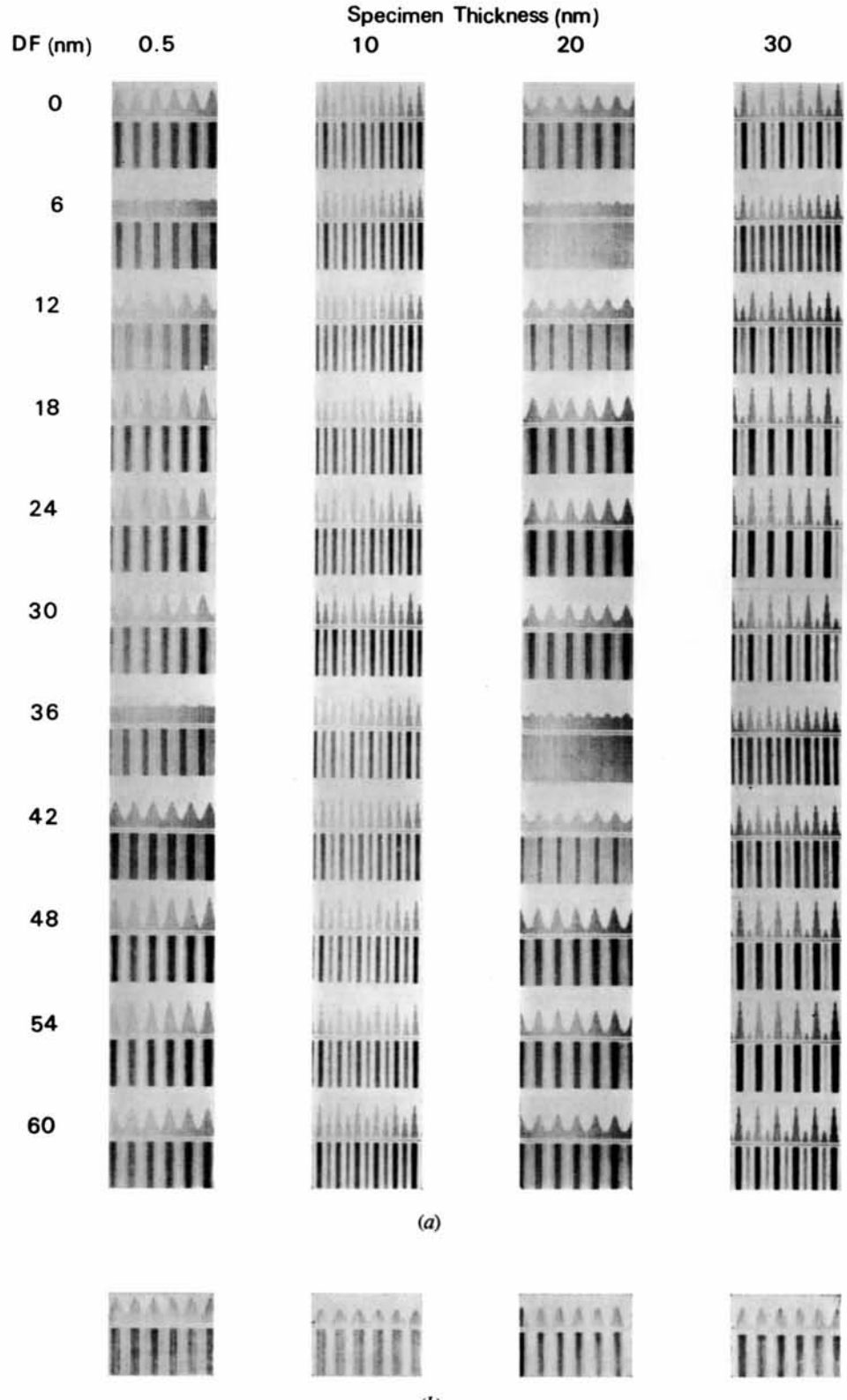

Fig. 3. Calculated lattice images for perfect, infinite graphite as a function of specimen thickness and objective lens defocus (DF). Images are shown for axial illumination (*a*) and the tilted illumination case (*b*).

[*To face p.* 826

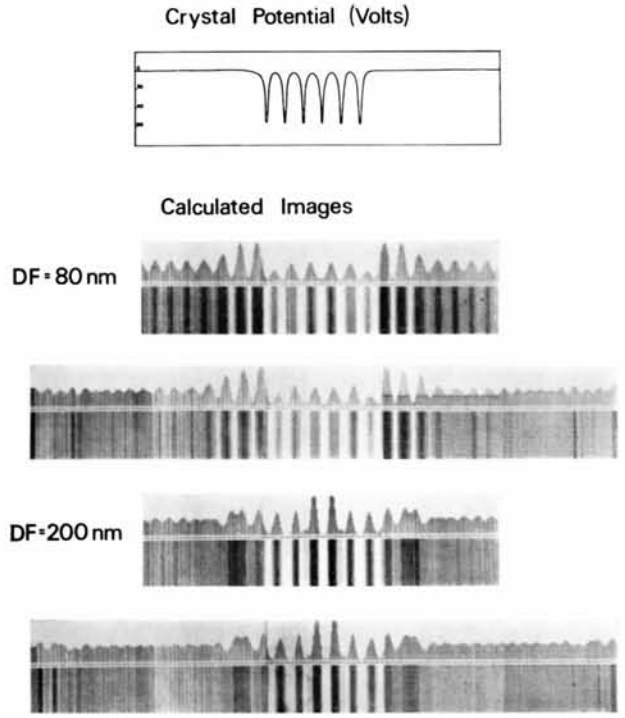

Fig. 5. Calculated lattice images of a six-layer crystal of graphite, computed on the basis of 66 and 110 Å unit cells, at different defocus values. The unit cell projected potential is indicated in each case.

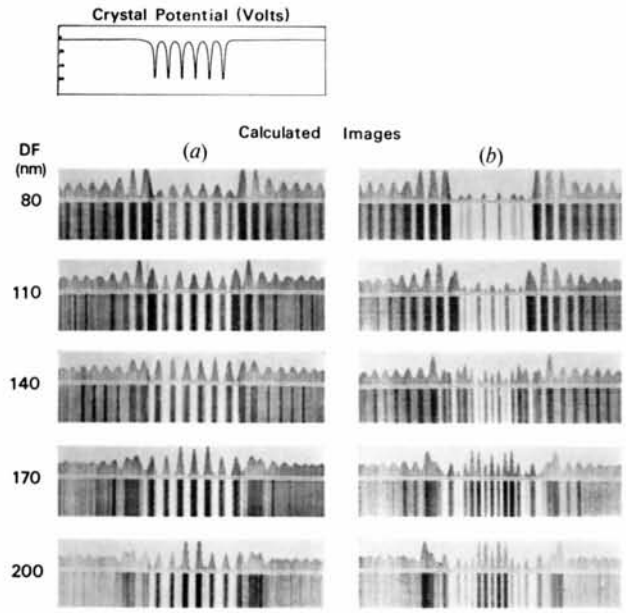

Fig. 6. Calculated lattice images of a six-layer crystal of graphite with DF ranging from 800 to 2000 Å in intervals of 300 Å. (*a*) specimen thickness 50 Å. (*b*) specimen thickness 100 Å. The images are plotted such that 3·4 Å fringes seen with the correct contrast will appear white. The crystal projected potential is shown for comparison.

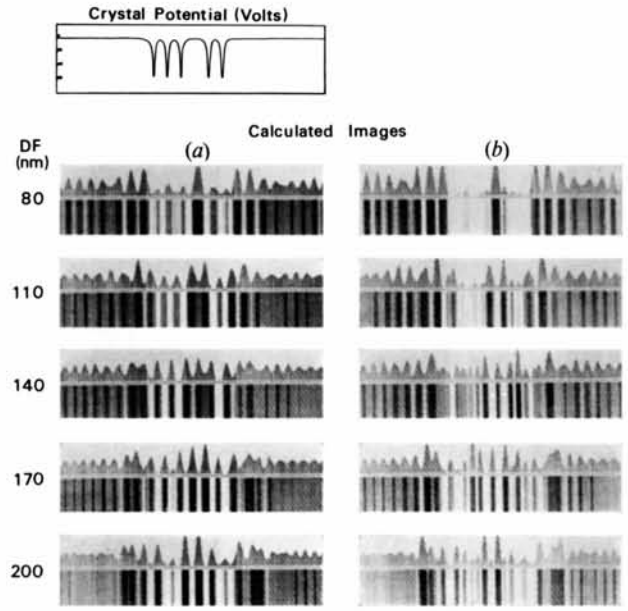

Fig. 7. The same crystal and the same conditions as for Fig. 6, but with one of the graphitic layers removed.

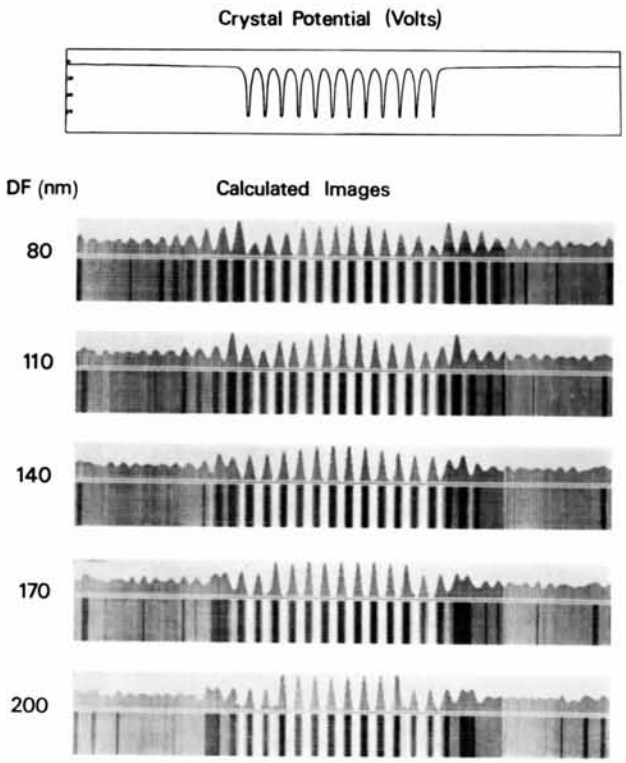

Fig. 8. A 12-layer crystal of graphite in a 110 Å unit cell, with images calculated at the same DF values as in Figs. 6 and 7, and a specimen thickness of 50 Å. The crystal projected potential is also shown.

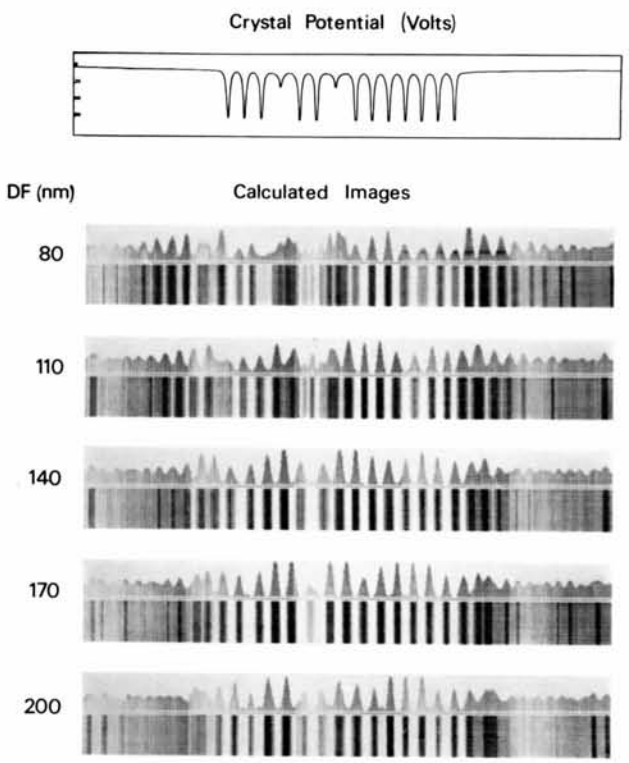

Fig. 9. The 12-layer crystal of Fig. 8, with two layers of intercalated potassium atoms, giving an overall stoichiometry of $C_{48}K$.

correspond to black fringes, and in the intercalated crystal only the six right-hand fringes are correctly indicated). The situation is similar at DF = 1100 Å but contrast is now reversed, the seven right-hand fringes having their correct positions, perturbations in the contrast appearing at the K positions, but the contrast of the remaining 3·4 Å fringes is severely affected. Subsequent increases in DF do nothing to simplify the image, and in each case it appears that a contrast reversal of the 3·4 Å fringes occurs at the positions of the intercalated K atoms. Although the calculated images are clearly perturbed in some way, it is difficult to deduce the precise nature of that perturbation without *a priori* knowledge of the positions of the K atoms. Further work upon models of this type is continuing, in an effort to try to simulate images of such intercalates reported recently (Evans & Thomas, 1975; Thomas, Evans, Davies & Millward, 1976).

3. Conclusions

The effects of increasing specimen thickness (and thereby increasing multiple scattering) upon images of graphitic carbons may be subdivided into two categories. In as far as the effect of multiple scattering upon 3·4 Å fringe contrast is concerned, the calculated images of perfect and infinite specimens provide the clearest indication. From these calculations it is evident that a weak-phase-object approximation is totally inadequate when the specimen thickness exceeds 50 Å. For thinner specimens, owing to the $\pi/2$ phase difference between 000 and 002 diffracted beams predicted by a simple three-beam theory and systematics multislice calculations, the weak-phase-object approximation will hold in at least a qualitative form. Indeed, if the thickness is less than 25 Å, the approximation can be applied quantitatively, but whether or not in practice specimens can routinely be made so thin remains to be discovered. For axial illumination, a simple three-beam dynamical theory is quite adequate to describe the scattering behaviour, but for cases of tilted illumination an extension of this or, alternatively, a multislice approach is required.

When the effect of multiple scattering upon the contrast variations due to crystal imperfections or finite crystal size is considered, the picture becomes less clear. Images calculated for such systems display the same variations in 3·4 Å fringe contrast as those predicted from infinite-crystal models: namely the emergence of a splitting of the 3·4 Å fringes into 1·7 Å components which becomes evident if the specimen thickness is greater than 50 Å. Contrast variations from imperfections, however, appear to be less severely affected. In particular, for a missing layer in the six-layer crystal model, the nature of the defect is shown equally well by the calculated images for specimen thicknesses of 50 and 100 Å at DF = 800 Å. However, at this value of DF, overall fringe contrast is rather poor. This suggests that the complex variation of image contrast at imperfections results more from spherical aberration and DF, coupled with the finite size of the crystals involved, rather than from multiple scattering effects. Support for this behaviour comes from the fact that at DF = 800 Å and $C_s = 1{\cdot}6$ mm beams corresponding to d spacings higher than 3·5 Å are transferred to the image plane in phase with the 000 beam. Since these are the beams which contain information regarding crystal size and perfection, we might therefore expect to observed the imperfections in their correct positions. This behaviour is also observed in the calculated images of the K-intercalated graphite. A reduction in 3·4 Å fringe contrast results from the beam corresponding to this spacing being transferred to the image slightly out of phase with the 000 beam.

The results of the calculations discussed above appear to support the findings of Cowley (1976) that in cases of materials containing planar defects, a kinematical treatment can be applied to the study of the defects even if the crystal shows strong multiple scattering, providing that the defects are not too closely spaced. This also implies that multiple scattering calculations of such defective systems may be readily carried out with the dynamical calculation for perfect crystals multiplied by an appropriate crystal size/perfection function. However, with specimens of graphitic carbons, all images will be severely affected by the transfer properties of the electron optical system. Some correction must therefore be made, and as all correction procedures to date assume that the specimen acts as a weak-phase object, the difficulties of applying such corrections are obvious.

This work has general consequences in the study of so-called paracrystalline carbons, *e.g.* certain heat-treated organic compounds which pass through the mesophase (Marsh, Augustyn, Cornford, Crawford & Hermon, 1975; Ban, Crawford & Marsh, 1975; White & Zimmer, 1976) prior to formation of pseudographitic material. Materials such as these correspond closely to some of the models discussed above, and consequently great care is necessary in the interpretation of micrographs of such systems, particularly as regards the crystal size and aspects of the overall perfection.

The authors thank the Computer Unit, University College of Wales, Aberystwyth, for computational assistance, and Mr J. Ll. Jenkins for preparing the figures. One of us (G.R.M.) received financial support from the Walter Idris Jones Fund and the National Coal Board and this is gratefully acknowledged. We also acknowledge the support of the Science Research Council.

References

BAN, L. L. (1972). *Surface and Defect Properties of Solids*, Vol. 1, p. 54. London: The Chemical Society.

BAN, L. L., CRAWFORD, D. & MARSH, H. (1975). *Proc. 12th Bienn. Conf. Carbon, Pittsburgh*, pp. 119–120.
COWLEY, J. M. (1976). *Acta Cryst.* A**32**, 83–87.
COWLEY, J. M. & MOODIE, A. F. (1957*a*). *Acta Cryst.* **10**, 609–619.
COWLEY, J. M. & MOODIE, A. F. (1957*b*). *Proc. Phys. Soc.* (*B*), **70**, 486–496.
CRAWFORD, D. & MARSH, H. (1975). *Proc. 12th Bienn. Conf. Carbon Pittsburgh*, pp. 115–116.
EVANS, E. L., JENKINS, J. LL. & THOMAS, J. M. (1972). *Carbon*, **10**, 637–642.
EVANS, E. L. & THOMAS, J. M. (1975). *J. Solid State Chem.* **14**, 99–111.
FOURDEUX, A., HERINCKX, C., PERRET, R. & RULAND, W. (1969). *C. R. Acad. Sci. Paris*, **269**, 1597–1600.
GRINTON, G. R. & COWLEY, J. M. (1971). *Optik*, **34**, 221–233.
HEIDENREICH, R. D., HESS, W. M. & BAN, L. L. (1968). *J. Appl. Cryst.* **1**, 1–19.
HINES, R. L., IMESON, D. & HOWIE, A. (1975). Unpublished.
HOERNI, J. A. (1956). *Phys. Rev.* **102**, 1534–1542.
JOHNSON, D. J. & CRAWFORD, D. (1973). *J. Microsc.* **98**, 313–324.
LYNCH, D. F. (1974). *Acta Cryst.* A**30**, 101–102.
MACLAGAN, D. S., BURSILL, L. A. & SPARGO, A. E. C. (1975). *Acta Cryst.* A**31**, S292.
MARSH, H., AUGUSTYN, D., CORNFORD, C., CRAWFORD, D. & HERMON, G. (1975). *Proc. 12th Bienn. Conf. Carbon, Pittsburgh*, pp. 117–118.
MILLWARD, G. R. & THOMAS, J. M. (1974). *Proceedings of the Fourth International Carbon and Graphite Conference, London.* In the press.
ROGERS, G. L. (1969). *J. Microsc.* **89**, 121–124.
SPENCE, J. C. H. (1975). *Proceedings of EMAG-75 Conference, Bristol, U.K.* In the press.
THOMAS, J. M., EVANS, E. L., DAVIES, N. C. & MILLWARD, G. R. (1976). To be published.
WHITE, J. L. & ZIMMER, J. (1976). *Surface and Defect Properties of Solids*, Vol. V. London: The Chemical Society. In the press.

Acta Cryst. (1976). A**32**, 828

Calculation of Lattice Sums and Heats of Sublimation of Long-Chain Even *n*-Alkanes

BY H. E. LUNDAGER MADSEN* AND R. BOISTELLE

Centre des Mécanismes de la Croissance Cristalline, Université d'Aix-Marseille III, *Centre Scientifique St. Jérome*, 13397 *Marseille, Cédex* 4, *France*

(*Received* 5 *February* 1976; *accepted* 10 *March* 1976)

Crystal energies at 0 K and 25 °C of three polymorphic forms of the normal alkanes $C_{28}H_{58}$ and $C_{36}H_{74}$ have been calculated from crystal structure data with a Lennard–Jones 6–12 potential. Taking into account the side packing and end packing energies, a general expression for the heat of sublimation at 25 °C has been derived, *viz* $\Delta H^0_{sub} = 8{\cdot}24n_C + 4{\cdot}10$ kJ mol^{-1}, where n_C is the number of C atoms in the molecule. The agreement with the two known experimental values (for $C_{18}H_{38}$ and $C_{32}H_{66}$) is within 1 %.

Introduction

In the search for an explanation of the observed growth kinetics of paraffin crystals growing from solution (Grassi, 1973; Simon, Grassi & Boistelle, 1974; Doussoulin, 1975; Boistelle & Doussoulin, 1976; Madsen, 1976*a*) we needed information about the energies of interaction of one molecule at some given position in the crystal with other molecules belonging either to the crystal or to the solution. For a molecule at the repeatable step the total energy (half-crystal energy) is closely related to the heat of sublimation which is, however, unknown for octacosane and hexatriacontane, the paraffins we have studied. Knowing the crystal structure and the potential energy of two molecules as a function of their separation we are able to calculate the half-crystal energy as well as other important interaction energies. Conversely, an independent knowledge of the heat of sublimation of some long-chain alkane of similar structure would provide us with a test of adequacy of the potential function used. Finally, we are interested in equilibrium shapes of crystals; these are deducible from surface energies which, in turn, may be calculated from appropriate lattice sums.

Structural features

Octacosane, $C_{28}H_{58}$, and hexatriacontane, $C_{36}H_{74}$, which are of particular interest to us, crystallize in several different crystal phases. The structures of monoclinic and orthorhombic phases of $C_{36}H_{74}$ have been determined by Shearer & Vand (1956) and by Teare (1959), respectively. The orthorhombic polytypic structure of $C_{28}H_{58}$ has been determined by Boistelle, Simon & Pepe (1976). From these three

* Present address: Chemistry Department, Royal Veterinary and Agricultural University, Thorvaldsensvej 40, 1871 Copenhagen V, Denmark.